ELSEVIER

Polymer 42 (2001) 1131–1142

polymer

www.elsevier.nl/locate/polymer

Structural changes of segmented copolyetheresteramides with uniform aramid units induced by melting and deformation

M.C.E.J. Niesten[a], S. Harkema[a], E. van der Heide[b], R.J. Gaymans[a,*]

[a]*Laboratory of Polymer Technology, Department of Chemical Technology, University of Twente, P.O. Box 217, 7500 AE Enschede, The Netherlands*
[b]*Shell Research and Technology Centre, Amsterdam, The Netherlands*

Received 16 March 2000; accepted 13 June 2000

Abstract

The structural changes induced by melting and deformation of segmented copolymers with uniform bisesteraramid units and poly(tetramethyleneoxide) (PTMO) based soft segments are investigated. With DSC, WAXS and IR it was shown that the uniform bisesteraramid units self assemble in the melt through the formation of hydrogen bonds. This leads to fast and nearly complete crystallization into lamellae with a thickness of only one bisesteraramid repeat unit (1.8 nm). IR-dichroism measurements showed that during the first 300% strain the bisesteraramid units preferentially orient transverse to the polymer chain direction, after which they become oriented in the polymer chain direction. This is attributed to the high aspect ratio of the thin aramid crystalline lamellae. The following model for the structural changes during deformation was proposed: first the bisesteraramid crystalline network is disrupted and the lamellae are, due to their high aspect ratio, preferentially oriented perpendicular to the polymer chain direction. At the same time, the bisesteraramid lamellae are broken up in their lateral dimension into eventually 'square' crystallites. These small crystallites are oriented parallel to the polymer chain direction. The orientation of the polymers was also studied with synchrotron WAXS measurements. After approximately 300% strain, the polyether phase strain crystallizes. The bisesteraramid orientation is irreversible while the PTMO orientation disappears upon strain release. $PTMO_{1000}$ based soft segments and PTMOm soft segments strain crystallize reversibly and PTMO segments longer than 1000 g/mol strain crystallize irreversibly.

Keywords: Segmented copolyetheresteramides; Bisesteraramid; Uniform

1. Introduction

In the previous studies the synthesis and properties of segmented copolyetheresteramides with crystallizable aramid units of uniform length were described extensively (TΦT–PTMO (poly(tetramethyleneoxide) — PTMO) Fig. 1) [1–3]. The TΦT units in TΦT–PTMO copolymers crystallize fast and nearly completely upon cooling from the melt even when present at low concentrations (3–29 wt%). The polymers possess a low glass transition temperature (−65°C), independent of the TΦT content. The rubbery plateau is temperature independent and the flow transition is sharp and high (102–248°C). This was explained by assuming that the uniform TΦT units crystallize nearly completely into lamellae of uniform thickness melting in a narrow temperature range. Furthermore, the fracture strain was found to be very high (1300–2000%) and the materials are highly elastic. Based on the model for the morphology of segmented copolyetheresters with crystallizable polyester hard segments introduced by Cella [4], the following morphology (Fig. 2) for TΦT–PTMO segmented copolymers was proposed. The TΦT units form crystalline lamellae of uniform thickness (C) acting as physical crosslinks for the amorphous PTMO phase (A). An additional PTMO crystalline phase is present if PTMO segments longer than 1000 g/mol are used. Although the TΦT units are extremely short (1.8 nm), they seem to crystallize easily. For poly(butylene terephthalate) it is known that the minimum PBT length to obtain a crystallizable PBT segment is 6 nm, corresponding to four PBT units [5], while for nylon-4,6 the minimum length is two repeat units [6]. The uniform TΦT units are expected to crystallize over their full length facilitating the ordering and hence the crystallization.

The aim of this study is twofold. In the first part a possible ordering of the TΦT units above the melting temperature of the TΦT–PTMO copolymers is studied with DSC, WAXS and IR. In the second part, the orientation behavior of the hard and soft segments is studied with IR-dichroism and synchrotron WAXS measurements.

* Corresponding author.
E-mail address: r.j.gaymans@ct.utwente.nl (R.J. Gaymans).

0032-3861/01/$ - see front matter
PII: S0032-3861(00)00452-3

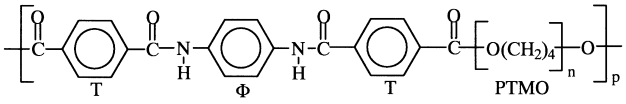

Fig. 1. Structure of segmented copolymer TΦT–PTMO.

IR-dichroism experiments were performed on unoriented, drawn and spindrawn fibers to follow the orientation of the amide and ether groups during the first 450% strain. The orientation was also followed with synchrotron WAXS measurements up to strains of 1800%. The influence of the structure of the PTMO phase on the orientation and the soft segment crystallinity is also investigated. The PTMO crystallinity is reduced by introducing structural irregularities in the PTMO chain, for instance by incorporating methyl side groups or by extending PTMO segments to longer PTMO blocks with dimethyl terephthate (DMT) or dimethyl isophthalate (DMI). In a previous publication it was shown that the presence of DMT or DMI units in the PTMO amorphous phase does not increase the T_g [2]. TΦT copolymers with the following types of PTMO were compared (Fig. 3).

1.1. Melting behavior

Aromatic polyamides often form lyotropic mesophases. Their melting temperature is generally too high to obtain a thermotropic mesophase. The melting temperature of TΦT–PTMO copolymers is much lower than of the aromatic polyamides self making these polymers melt processable. The question remains whether the TΦT units form a liquid crystalline phase.

Sek et al. [7] observed a liquid crystalline phase for alternating polyesteramides based on uniform aromatic amide triads and 1,10-decanediol.

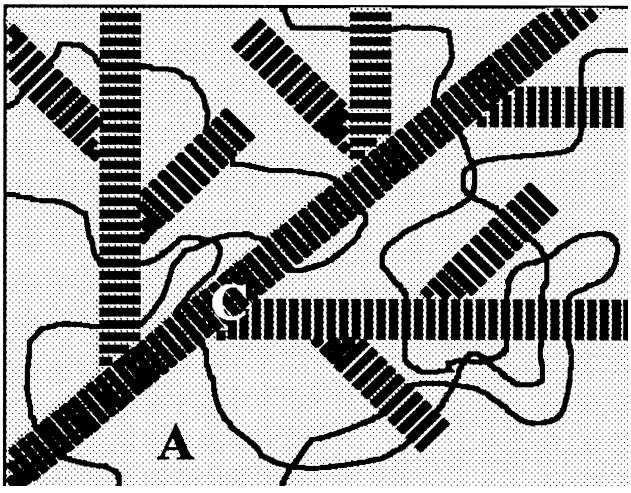

Fig. 2. Schematic representation of morphology of TΦT–PTMO segmented copolymers: (C) crystalline TΦT lamellae of uniform thickness; (A) amorphous PTMO phase.

Lenz [8] studied thermotropic liquid crystal copolyetheresters. The mesogenic units, composed of aromatic ester triads were coupled by aliphatic poly(oxyethylene) spacers. If the length of the poly(oxyethylene) spacer (n) is smaller than 9 ($M < 400$ g/mol) both nematic and smectic phases were formed. Using a poly(oxyethylene) spacer with $n = 13.2$ ($M = 600$ g/mol), no liquid crystalline phase was observed. This was explained by the increased mobility of the long spacers compared to the short spacers, rendering higher degrees of freedom to the mesogenic units which permits easy packing into the crystalline lattice. Similar results were obtained by Kricheldorf et al. [9] who investigated polyesterimides with uniform imides coupled by flexible aliphatic spacers. For these polymers with spacers of more than 12 CH_2-groups, Wutz [10] proposed a smectic crystalline phase, i.e. the uniform imide units undergo lateral interactions giving rise to WAXS reflections, while no ordering was observed in the polymer chain direction. It is expected that TΦT–PTMO copolymers containing PTMO segments of 650 g/mol and longer crystallize too fast to form a liquid crystalline phase.

1.2. Morphology during deformation

In the 1960s Bonart [11] studied the changes in the morphology of segmented polyurethanes upon straining. The soft segments are stretched thereby exercising forces on the crystalline domains. Strain induced crystallization of the soft segments started at about 150% strain. Up to about 200% strain, the crystalline network of the hard phase is disrupted and the soft segments are oriented. Above 200% strain, the X-ray reflection of the polyurethane hard segments moved to the meridian, which means that during the first 200% strain the crystalline polyurethane lamellae are preferentially oriented perpendicular to the polymer chain direction while at higher strains they are oriented parallel to the polymer chain direction. Eventually, the original crystalline lamellae are broken up into very small crystalline units.

Later, several studies using IR-dichroism to investigate the orientation of segmented non-hydrogen bonding polyurethanes [12], segmented copolymers with hydrogen bonding polyurethanes [13,14] and segmented copolymers with poly(butylene terephthalate) segments [15] confirmed this model. These studies showed that crystalline lamellae initially tend to orient transverse to the polymer chain direction, although the transverse orientation was quite small. After about 50% strain, the orientation became positive and hence from there the crystals orient into the polymer chain direction. Amorphous hard segments were found to orient parallel to the polymer chain direction from the beginning. The initial transverse orientation of the crystalline lamellae was attributed to their high aspect ratio. Furthermore, these studies showed that the soft segments relax upon load release, while the hard segments remain oriented.

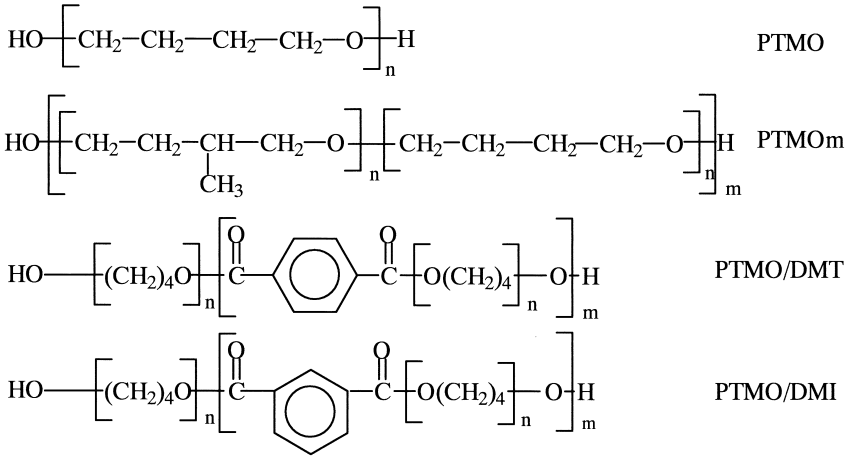

Fig. 3. Structure of different types of PTMO.

2. Experimental

2.1. Polymerization

The polymers were synthesized according to polymerization route I described in a recent publication [1].

2.2. Sample preparation

2.2.1. Spinning and drawing

On a small scale, fibers were melt spun by extruding a polymer on a 4cc DSM res RD11H-1009025-4 corotating twin screw mini extruder. The extruder temperature was varied from 30 to 90°C above the flow temperature of the polymer, while the screw speed was kept constant at 30 rpm. The fibers were winded at a speed ranging from 20–50 m/min.

The unoriented, as spun fibers were drawn on a Zwick Z020 universal tensile machine equipped with a 10 N load cell, the strain being measured as the clamp displacement. Samples were drawn by applying the desired draw ratio at a strain rate of 200 mm/min and releasing the strain after 5 min. The draw ratio was defined as:

$$\text{draw ratio} = \frac{\lambda_1}{\lambda_0} - 1 \ [-] \tag{1}$$

where $\lambda_0 =$ strain without drawing $(=1)$ [–] and $\lambda_1 =$ strain at desired draw ratio [–].

2.2.2. Spindrawing

On a semi-industrial scale, fibers were melt spun on an 18 mm single screw extruder nr. 524 at Acordis Research in Arnhem, the Netherlands. The screw speed of the extruder was 50–60 rpm. The flow of the polymer melt through the extruder was approximately 11 g/min. A spinneret with a diameter of 60 mm with ten 400 μm holes was used. Before the spinneret a filter was placed with 60–120–325–120–60 mazes/square inch. To avoid sticking of the fibers avivage (18 wt%) was spread on the fibers. The fibers were winded at a speed ranging from 100 to 400 m/min.

2.3. DSC

DSC spectra were recorded on a Perkin–Elmer DSC7 apparatus, equipped with a PE7700 computer and TAS-7 software. 2–5 mg of dried polymer sample was heated at a rate of 20°C/min. The first cooling and second heating scan were used to determine the melting and crystallization peaks. The peak maximum or minimum was used as the melting or crystallization temperature, respectively, the peak area as the enthalpy.

2.4. FTIR as function of temperature

Infrared (IR) transmission spectra were recorded using a Nicolet 20SXB FTIR spectrometer with a resolution of 4 cm^{-1}. Samples of polymer $(T\Phi T–PTMO_{1000}/DMT)_{2000}$ were solution casted from phenol/1,1,2,2-tetrachloroethane (50/50 mol%) on a pressed KBr tablet. Before starting the measurements the sample was heated to 200°C and cooled down to room temperature to obtain a polymer film crystallized from the melt. The IR spectra were recorded at several temperatures between room temperature and 250°C.

2.5. Infrared dichroism

The orientation of different groups in unoriented, drawn and spindrawn melt spun fibers was measured with IR dichroism [16]. For the amide unit, the amide and ester carbonyl groups were measured, for the polyether, the ether group. In Table 1 the band assignment of these groups and the angle α between the transition moment of the selected absorbing group and the chain axis is given. For uniaxial orientation, the degree of orientation can be expressed by the following Hermans orientation function:

$$f = \frac{3\langle \cos^2 \beta \rangle - 1}{2} \ [-] \tag{2}$$

Table 1
IR band assignments and bond angle α [17] with the chain

Frequency [cm^{-1}]	Assignment	Angle α (°)
1715	C=O stretching, aromatic ester	78
1647	C=O stretching, amide	78
1098	C–O–C stretching	0

where β is the angle between the chain axis and the deformation axis. For unoriented chains, f equals 0, for perfectly uniaxially chains, f equals 1 and for perpendicular orientation f equals -0.5.

In addition, f is related to the dichroic ratio (R) and the transition moment angle α (Eq. (3))

$$f = \frac{(R-1)(R_o+2)}{(R_o-1)(R+2)} \quad [-] \tag{3}$$

The dichroic ratio (R) is calculated according to the following equation

$$R = \frac{A_{parallel}}{A_{perpendicular}} \quad [-] \tag{4}$$

in which A is the absorption. R_o, the dichroic ratio for perfect uniaxial orientation, is given by the following equation

$$R_o = 2\cot^2 \alpha \quad [-] \tag{5}$$

where α is the angle between the transition moment of the selected absorbing group and the chain axis. In Table 1 α is given for the different groups.

IR spectra were recorded with a resolution of 4 cm^{-1} using a Spectra-Tech IR PLAN microscope coupled to a Nicolet Magna 550 Fourier transform IR spectrometer, with a resolution of 4 cm^{-1}, co-adding 1000 scans. Attenuated Total Reflection (ATR) measurements were carried out using the ATR objective of the IR microscope, which contained a zinc selenide (ZnSe) crystal. Polarized light (1200 line/mm ZnSe wire grid polarizer) IR spectra are recorded at 0 and 90° with the fiber in the tensile direction. The measurement is repeated at the same spot after rotating the sample 90°.

2.6. X-ray diffraction as function of temperature

Diffraction patterns at different temperatures were obtained with a Philips X'Pert-MPD diffractometer, using a Cu-curved monochromator with a radiation of 1.5418 Å. Melt pressed samples of approximately 0.5 mm thickness were mounted in a sample holder in an Anton Paar HTK-16 temperature chamber. The measurements were carried out in a nitrogen atmosphere at temperatures ranging from 25 to 250°C.

2.7. Synchrotron WAXS

Synchrotron wide angle X-ray scattering (WAXS) measurements were performed on unoriented melt spun polymer fibers during straining at a straining rate of $10^{-2}\ s^{-1}$ and during stress relaxation of drawn fibers (750% pre-strained) at 200% strain at the ESRF in Grenoble (France) on ID11 [18]. The wavelength of the beam was 1.00 Å. Every 30 s a measurement was done with an exposure time of 10 s. The orientation was quantified by determining the half-width of the angular intensity distribution curve and calculated with the following equation

$$O = \frac{180}{A} \quad [-] \tag{6}$$

in which A is the half width in degrees.

3. Results and discussion

3.1. Melting behavior of the TΦT units

The melting behavior of the TΦT units in the polymers was studied with DSC, WAXS and IR. With DSC only small TΦT melting and crystallization peaks were observed at TΦT concentrations higher than 22 wt% and a liquid crystalline phase was not detected. The TΦT crystals are not visible with the polarized light microscope. WAXS pictures, however, showed the presence of a crystalline aramid phase. Oriented polymer samples possess aramid crystalline reflections on the equator (perpendicular to the polymer chain direction). On the meridian (parallel to the polymer chain direction) no TΦT reflections were observed. These results suggest that the short TΦT units (1.8 nm) form extremely thin crystalline lamellae giving rise to a WAXS reflection only in the lateral dimension. In the polymer chain direction the number of TΦT repeat units is one and consequently no reflections are observed in this direction. This type of ordering is sometimes called smectic-crystalline [10].

In Table 2 the DSC results of TΦT–PTMO copolymers are shown. The undercooling ($T_m - T_c$) is lower than 30°C, suggesting that the TΦT units crystallize extremely fast. For poly(butylene terephthalate), a fast crystallizing polymer, the undercooling is 36°C [19]. The melting temperature of the polymers is quite high, while the melting enthalpy is low. As $\Delta S_m = \Delta H_m/T_m$ the melting entropy is rather

Table 2
DSC results of TΦT phase in unoriented TΦT–PTMO copolymers

Polymer	TΦT content (wt%)	T_m (°C)	ΔH_m (J/g)	ΔH_m (J/g TΦT)	T_c (°C)	$T_m - T_c$ (J/g)
TΦT–$PTMO_{650}$	29	266	12	41	238	28
TΦT–$PTMO_{1000}$	22	222	10	45	203	18

small, suggesting that some kind of ordering of the TΦT units already exists in the melt.

To study whether the TΦT units order in the melt WAXS and IR measurements as function of temperature were carried out. In Fig. 4 the WAXS curves of TΦT–$(PTMO_{1000}/DMT)_{2000}$ at different temperatures (25–250°C) are shown. In the unoriented polymer, the polyether ($PTMO_{1000}$/DMT) segments are expected to be completely amorphous at room temperature [2]. In Fig. 4 only one, rather broad peak is visible which is broadened with increasing temperature and shifted to a lower angle (higher *d*-spacing) without disappearing. This peak probably originates from the amorphous PTMO phase. The crystalline aramid reflections might be hidden under this peak. According to the cell dimensions of aramid reported by Northolt [20], in this region the aramid peaks corresponding to the following *d*-spacings: 5.21 Å (010), 4.35 Å (110) and 3.94 Å (200) might be present. For the TΦT model compound *N*,*N*′-(*p*-phenylene)dibenzamide the following *d*-spacings were given at $d = 5.25$, 4.39 and 4.01 Å [21] agreeing well with the values reported by Northolt. Since the polyether phase dominates, no evidence of TΦT ordering in the melt is obtained from Fig. 4. However, also no proof of the absence of ordering is given. TΦT ordering in the melt could be caused by hydrogen bonding of the amide groups. The presence of hydrogen bonds in the melt was therefore studied with IR experiments.

The typical IR-bands of polyamides reported in the literature are summarized in Table 3. Skrovanek [22] attributes the broadness of the hydrogen bonded N–H stretch peak (3310 cm^{-1}) to a distribution of hydrogen bond strengths, i.e. a longer hydrogen bond length corresponds to a higher frequency. With increasing temperature, the hydrogen bond becomes weaker, leading to a lower absorption coefficient and hence the peak intensity is lowered. He concluded that the decrease of the peak intensity with temperature is mainly caused by this decrease of the absorption coefficient.

In Fig. 5a and b, the IR spectra at different temperatures of TΦT–$(PTMO_{1000}/DMT)_{2000}$ are shown. Fig. 5a gives the N–H stretching region (3100–3600 cm^{-1}), Fig. 5b the amide I and amide II region (1500–1750 cm^{-1}). In Fig. 5a the peak at 3333 cm^{-1} (hydrogen bonded N–H stretch) becomes weaker and broader with increasing temperature. At 190°C (approximately at the melting temperature [2]), the peak is very weak but still present and even at 250°C it has not disappeared completely. A tail seems to develop at the higher frequency side. In accordance with Skrovanek, these results suggest that the hydrogen bonds are still partly present in the melt. In Fig. 5b the peak at 1648 cm^{-1} (hydrogen bonded C=O) becomes smaller with increasing temperature without disappearing completely. The appearance of the peak at 1684 cm^{-1} (free C=O) suggests that some hydrogen bonds are destroyed by increasing the temperature. The peak at 1546 cm^{-1} (amide II) becomes

Table 3
IR bands assignments of amide groups in polyamides

Frequency (cm^{-1})	Description
3444 (weak) [22]	Free N–H
3310 (broad) [22]	Hydrogen bonded N–H stretch
1685 [23]	Free C=O
1640 [22]	Hydrogen bonded C=O stretch, amide I
1545 [22]–1529 [23]	Amide II, N–H in place deformation vibration

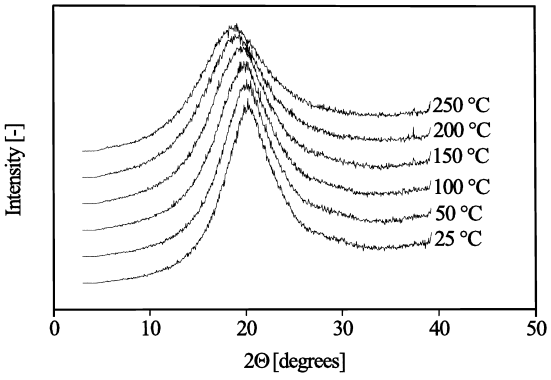

Fig. 4. WAXS curves (wavelength: 1.5418 Å) of unoriented injection molded sample of TΦT–$(PTMO_{1000}/DMT)_{2000}$ ($T_m \approx 190$°C) at different temperatures.

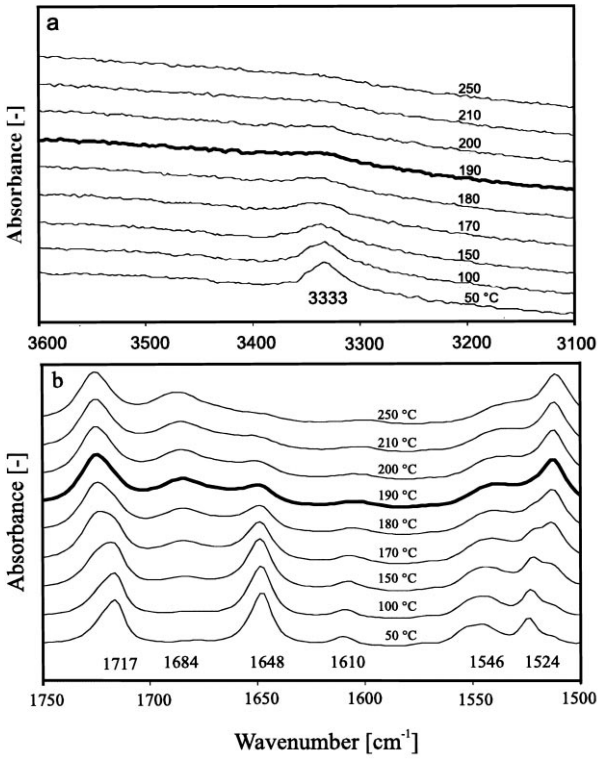

Fig. 5. IR spectra of TΦT–$(PTMO_{1000}/DMT)_{2000}$: (a) N–H stretching region; and (b) amide I and II region.

weaker and the peak at 1524 cm^{-1} (amide II, N–H in plane deformation vibration) shifts to a lower frequency with increasing temperature which is consistent with the decrease of the average hydrogen bond strength. The above described IR experiments confirm the idea that the TΦT units self assemble in the melt through the formation of hydrogen bonds into a possible smectic crystalline phase. Due to this self-assembling in the melt, the units easily order into the crystalline lattice giving only a small change in entropy. Contrary to what is often believed, the high melting temperature of the amides is mainly caused by their low melting entropy instead of a high melting enthalpy [24].

3.2. IR-dichroism

The orientation of the TΦT units and the PTMO segments during the first 450% strain was followed with IR-dichroism. The amide carbonyl stretching (1645 cm^{-1}), the aromatic ester carbonyl stretching (1715 cm^{-1}) and the C–O–C stretching (1098 cm^{-1}) were measured during straining. In Fig. 6a the amide carbonyl orientation functions are given versus the applied strain for TΦT–$PTMO_{1000}$, TΦT–$PTMO_{2000}$, TΦT–$(PTMO_{1000}/DMT)_{2000}$ and TΦT–$(PTMO_{1000}/DMI)_{2000}$, in Fig. 6b the corresponding ether and ester carbonyl orientation functions are shown. Theoretically, an unoriented group has an orientation function (f) of 0, a perfectly uniaxially oriented group has an orientation function of 1 and a group that is oriented perpendicular to the tensile direction has an orientation of −0.5. In Fig. 6a, however, orientation function values lower than −0.5 are observed. Moreland and Wilkes also observed orientation function lower than −0.5 for segmented polyurethanes [14]. The IR-dichroism measurements were carried out on the fiber surface according to the ATR technique. Maybe, at the fiber surface the orientation of the crystalline amides is biaxial instead of uniaxial. In certain cases of biaxial orientation, the lower limit of the orientation function (Eq. (2)) approaches minus one [21]. Transmittance IR-dichroism measurements should be carried out to verify this.

The starting value of the orientation function of the amide carbonyl groups is in all cases negative, indicating that during melt spinning already some orientation occurred. During the first 300% strain the amide carbonyls have a negative orientation function, which means that the crystalline TΦT lamellae are oriented with their lateral (= long) dimension in the tensile direction. Apparently the aspect ratio of the TΦT-lamellae is so large that at low strains they are preferentially oriented transverse to the polymer chain direction. The degree of negative orientation is higher than reported in literature [12–15]. A reason for this might be the high aspect ratio of the thin TΦT lamellae which favors perpendicular orientation. Another reason might be that at the surface the TΦT crystalline phase is biaxally oriented. Furthermore, in the other studies segmented copolymers with partly crystallizable hard segments were used [12–15]. A major part of the carbonyl groups in those polymers was present in the amorphous phase and consequently the negative orientation function of the crystalline carbonyl is partly counteracted by the positive orientation function of the amorphous carbonyl groups. At about 300% strain, the orientation function of the amide carbonyl groups goes up, eventually resulting in positive orientation functions, which means that from there, the TΦT lamellae are starting to become oriented in the polymer chain direction with the long dimension perpendicular to the polymer chain direction. This process is similar to the deformation process of segmented polyurethanes as described by Bonart [11]. In Fig. 7 a model is proposed for the structural changes that occur upon straining in TΦT–PTMO copolymers. During deformation three processes occur. First the crystalline network is disrupted and the crystalline lamellae are broken up in the lateral direction into smaller lamellae. At the same time, the lamellae are preferentially oriented transverse to the polymer chain direction due to their high aspect ratio. Upon further straining the lamellae are broken up further, eventually reaching ‘square’ dimensions and they orient parallel to the polymer chain direction. Above 300% strain, the polyether segments start to strain crystallize.

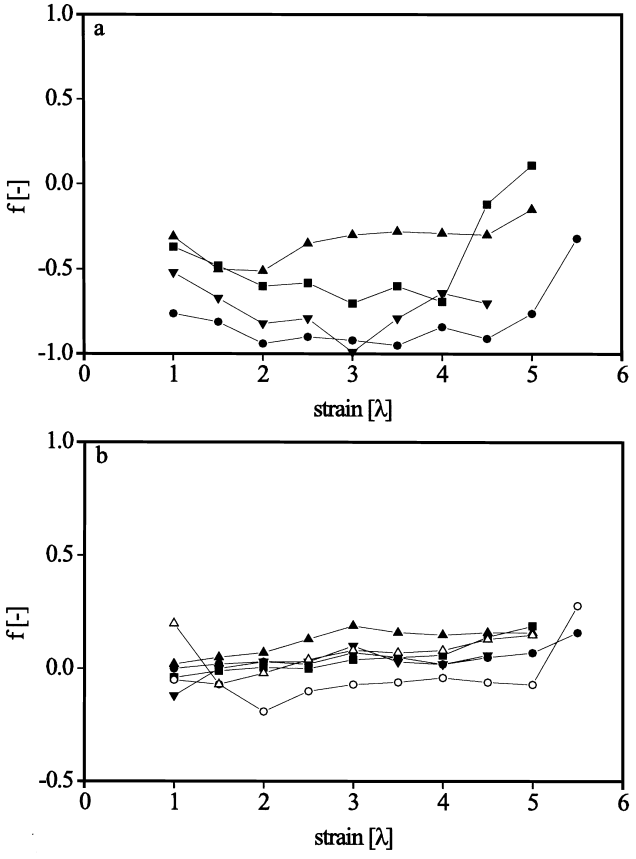

Fig. 6. Orientation function f during the first 450% strain of — (a) the amide carbonyl; and (b) the ethers (solid symbols) and the ester carbonyl (open symbols) for (●,○): TΦT–$PTMO_{1000}$, (▲,△): TΦT–$PTMO_{2000}$,(▼): TΦT–$(PTMO_{1000}/DMT)_{2000}$ and (■): TΦT–$(PTMO_{1000}/DMI)_{2000}$.

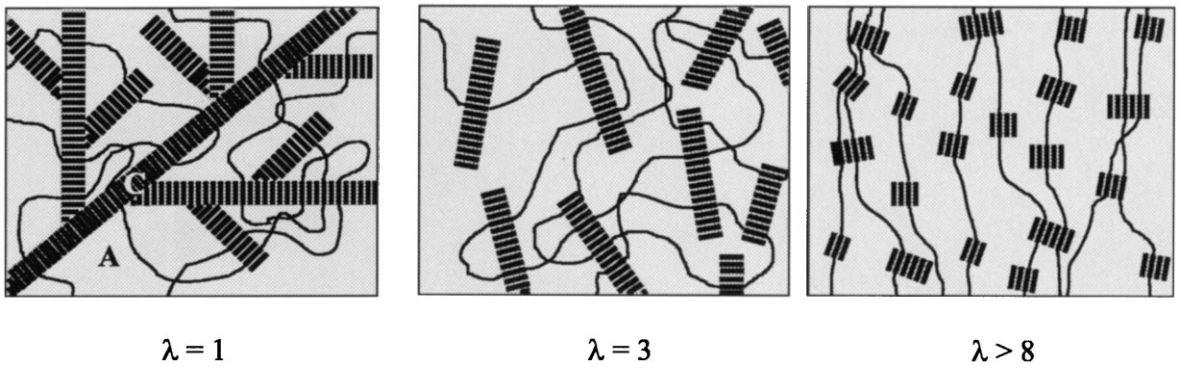

Fig. 7. Schematic representation of structural changes upon straining for TΦT–PTMO copolymers.

Fig. 6b shows that the ester carbonyl and ether groups have a similar orientation function. Therefore, it can be concluded that the ester carbonyl group orientation direction is similar to the polyether and different from the amide. The assumption made so far, that the TΦT units are only 1.8 nm long (carbonyl ester groups excluded) is thus valid. The ether groups (PTMO) are hardly oriented during the first 450% strain and no difference between the different types of PTMO was observed.

The effect of drawing and spindrawing of the fibers on the orientation functions for TΦT–$PTMO_{2000}$ and TΦT–$(PTMO_{1000}/DMI)_{2000}$ are shown in Fig. 8. The amide carbonyl groups are oriented positively after drawing and spindrawing, the degree of orientation being equal for both types of drawing. During drawing to 750% the TΦT units are oriented in the tensile direction and this orientation is not lost upon release of strain. The ether groups, on the other hand, hardly possess a higher orientation after drawing or spindrawing than the ether groups of the undrawn fibers. Therefore it can be concluded that for the first 450% strain the ether orientation induced by drawing is, at least, partly lost upon release of strain.

3.3. Synchrotron WAXS

Synchrotron WAXS measurements were carried out during tensile deformation on unoriented fibers or oriented (drawn) fibers. As an example, WAXS pictures of TΦT–$(PTMO_{1000}/DMT)_{2000}$ at different strains (a)–(c) and after drawing to 1000% (d) are shown in Fig. 9. At 129% strain, only rings are visible and hence hardly any orientation has occurred yet. At 600% strain, reflections have developed on the equator and these reflections are intensified upon further straining. No reflections are observed on the meridian indicating that no TΦT ordering in the polymer chain direction exists. The black spots on the equator probably originate from the mainly strain crystallized PTMO phase. The crystalline structure of the homopolymer PTMO is known to be monoclinic with main WAXS reflections at $d = 4.46$ Å ($2\Theta = 13°$, 020), $d = 3.66$ Å ($2\Theta = 15.7°$, 110) and $d = 2.38$ Å ($2\Theta = 24.3°$, 130) [25]. In the polymers these PTMO reflections have a d-spacing of 4.4 Å ($2\Theta = 13°$), 3.8 Å ($2\Theta = 15.1°$) and 2.3 Å ($2\Theta = 24°$), respectively. The weaker reflections at the inner and outer side of the PTMO ring are probably the TΦT reflections ($d = 5$ Å: $2\Theta = 11.5°$ and $d - 3.2$ Å: $2\Theta = 18°$). According to the cell dimensions of aramid reported by Northolt [20], in this region the aramid reflections corresponding to the following d-spacings: 5.21 Å (010), 4.35 Å (110) and

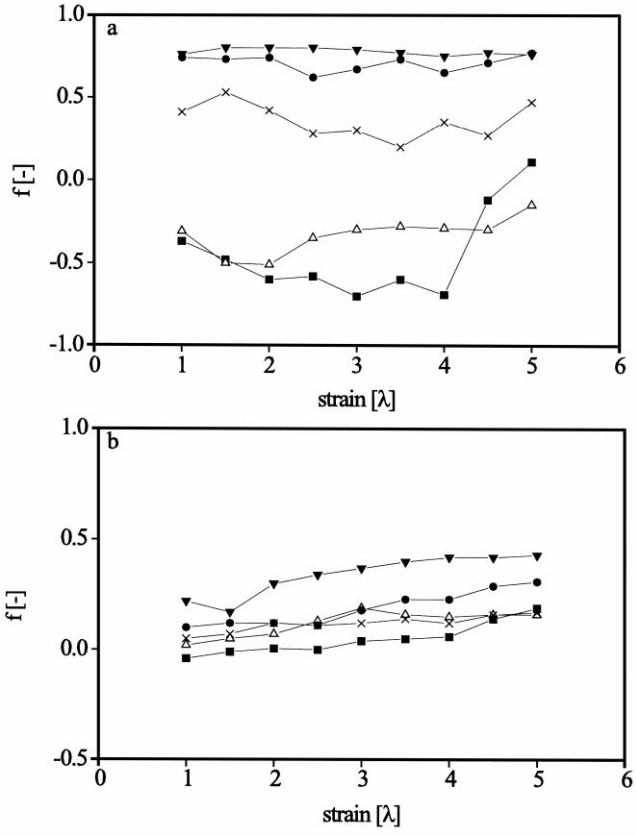

Fig. 8. Effect of drawing (750%) and spindrawing (350 mm/min) on the orientation function of — (a) the carbonyl amides; and (b) the ethers for (△): TΦT–$PTMO_{2000}$, (▼): TΦT–$PTMO_{2000}$ drawn to 750%, (●): TΦT–$PTMO_{2000}$, spindrawn, (■): TΦT–$(PTMO_{1000}/DMI)_{2000}$ and (×): TΦT–$(PTMO_{1000}/DMI)_{2000}$ spindrawn.

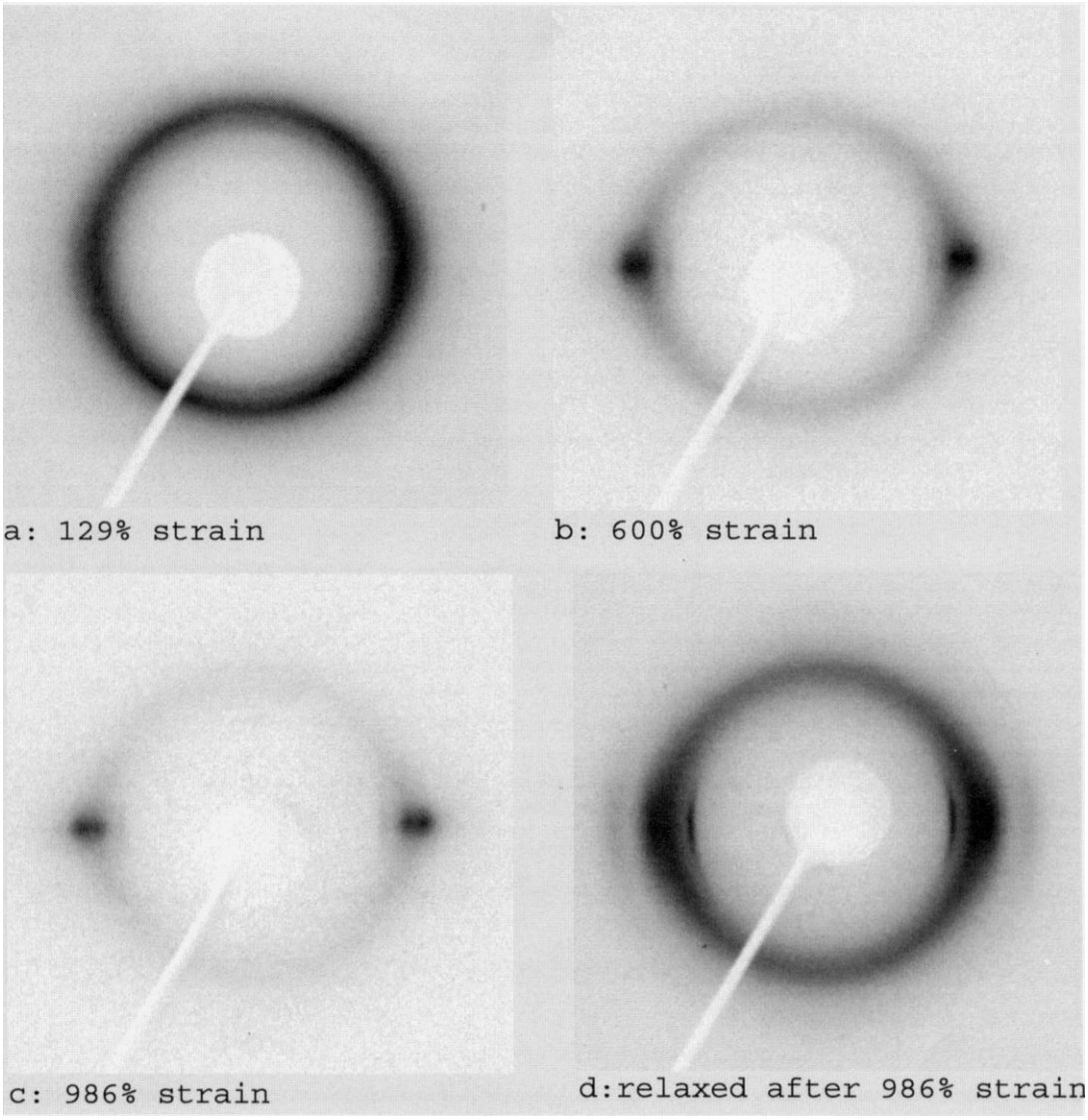

Fig. 9. WAXS of TΦT–$(PTMO_{1000}/DMT)_{2000}$ (a), (b) and (c) during straining and (d) after relieving the strain (wavelength: 1 Å).

3.94 Å (200) might be present. For the TΦT model compound *N*,*N*′-(*p*-phenylene)dibenzamide the following *d*-spacings were given at $d = 5.25$, 4.39 and 4.01 Å [21] agreeing well with the values reported by Northolt. Yamada et al. [26] incorporated TΦT in poly(ethylene terephthalate) and observed reflections at $d = 5.21$, 4.35 and 3.94 Å. In the TΦT–PTMO copolymers the investigation of the TΦT crystalline reflections is hindered by the PTMO strain induced crystallinity which gives reflections at $d = 4.4$ Å and $d = 3.8$ Å, overlapping the TΦT reflections. As an example, 2Θ scans of the equator of TΦT–$PTMO_{1000}$ and TΦT–$(PTMO_{1000}/DMT)_{2000}$ at different strains are shown in Fig. 10.

In pre-strained (drawn) fibers the PTMO chains are relaxed and the crystallization is (partly) lost. Consequently, after relieving the stress (Fig. 9d), the PTMO orientation is deceased as well as the intensity of the PTMO peaks compared to TΦT reflections. The TΦT reflections at $d =$ 5 Å and $d = 3.2$ Å (inner and outer reflection) are now more pronounced than in Fig. 9a–c. During the test, the intensity of the X-ray beam decreased, and therefore not too much importance should be attached to the absolute value of the intensity. At approximately 100% strain ($\lambda = 2$), one broad peak is visible which splits up upon straining.

With IR-dichroism it was observed that the TΦT units tend to orient perpendicular to the polymer chain directions during the first 300% strain after which they tend to become oriented parallel to the polymer chain direction. In the WAXS picture (Fig. 9) this should result in a shift of the 010 ($d = 5$ Å) reflection from the meridian to the equator. The reflection belonging to the lamellar thickness (100) is not visible as there is no ordering of the TΦT units in the polymer chain direction. The lateral reflections ($d = 5.0$ Å, $2\Theta = 11.5°$ and $d = 3.2$ Å, $2\Theta = 18.0°$) are visible and they become somewhat more pronounced in the 2Θ scan of the equator after 100% strain ($\lambda = 1.9$, Fig. 10a). In the

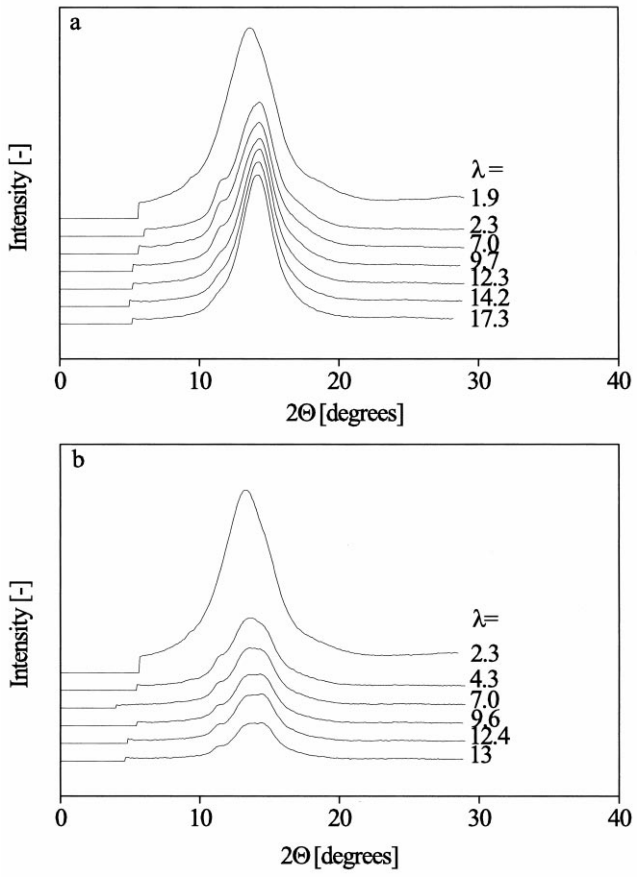

Fig. 10. 2Θ scan of the equator at different strains of: (a) TΦT–$PTMO_{1000}$; and (b) TΦT–$(PTMO_{1000}/DMT)_{2000}$.

unoriented polymer, one ring is found and the separate rings are hard to distinguish. Therefore, it cannot be excluded that reflections of the lateral dimension of the TΦT lamellae are shifted to the equator at strains above 100%. The 010 aramid ($d = 5$Å) reflection is too weak to determine the orientation of the TΦT units.

3.4. The effect of strain on the PTMO crystallinity

The PTMO crystallinity induced by straining was studied with DSC and synchrotron WAXS. In Fig. 11 a DSC diagram of unoriented and oriented (1000% pre-strained) melt spun fibers of TΦT–$PTMO_{1000}$ and TΦT–$PTMO_{2000}$ are shown. The PTMO melting peaks are indicated by arrows. On orienting TΦT–$PTMO_{2000}$, the PTMO melting temperature peak sharpens and shifts to a higher temperature ($-3 \rightarrow 45$°C). The increase of the melting temperature due to straining is caused by changes in the free energy of the crystalline and amorphous phase [27,28]. Schematically, this phenomenon is illustrated in Fig. 12. If the polymer is strained, both the amorphous and crystalline free energy of the PTMO phase increase. The crossing point of these two curves, the melting temperature, also increases. After releasing the strain, the melting temperature is lowered again, but

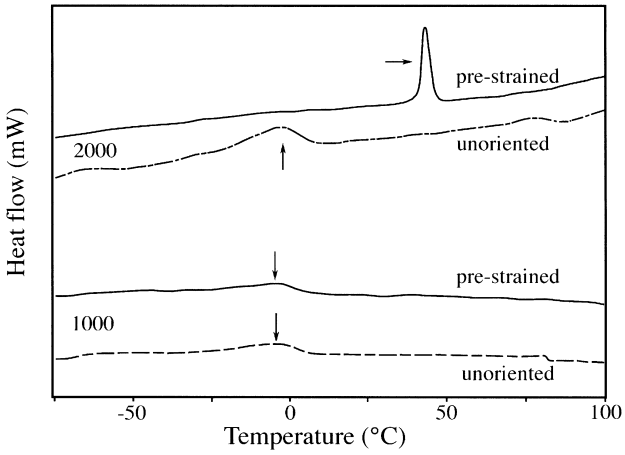

Fig. 11. PTMO melting peaks of unoriented and 1000% pre-strained TΦT–$PTMO_{1000}$ and TΦT–$PTMO_{2000}$.

as long as the increased melting temperature during straining is far above room temperature, the melting temperature of the oriented and unstrained PTMO will remain above room temperature.

The $PTMO_{1000}$ melting peak is broad and below 0°C, no difference between the melting peak of the unoriented and the oriented sample is observed (Fig. 12). This suggests that the melting temperature of strain induced crystallized $PTMO_{1000}$ is just above room temperature during straining. Hence, after releasing the strain the melting temperature shifts to a temperature below room temperature and consequently the strain induced PTMO crystals melt.

Synchrotron WAXS measurements of TΦT–$PTMO_{1000}$ threads taken during straining, clearly show the presence of a $PTMO_{1000}$ crystalline phase, although less crystalline than TΦT–$PTMO_{2000}$. The differences in PTMO crystallinity at 1000% strain between the polymers with different types of PTMO is visible in an equatorial 2θ scan of the WAXS pictures. In Fig. 13, equatorial 2θ scans of several polymers strained to 1000% is shown. Again, it

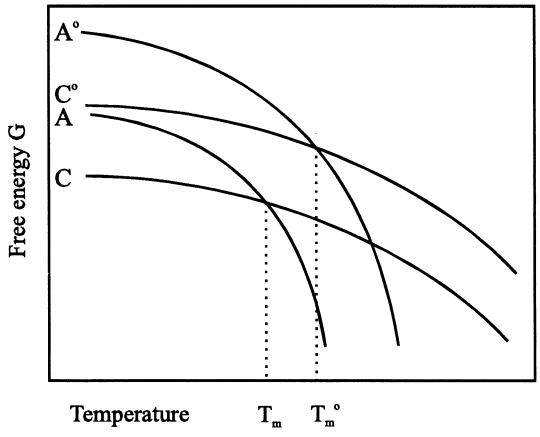

Fig. 12. Schematic representation of increase of melting temperature upon straining due to changes in the free energy G of the crystalline (C) and amorphous (A) PTMO phases, superscript o means oriented.

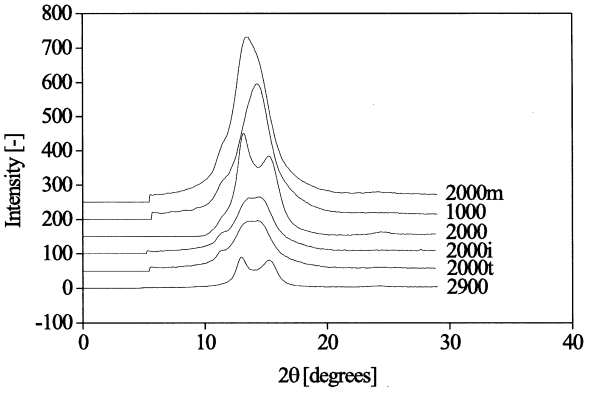

Fig. 13. 2θ scans at 1000% strain for: (1000) TΦT–$PTMO_{1000}$; (2000) TΦT–$PTMO_{2000}$; (2900) TΦT–$PTMO_{2900}$; (2000(1000)t) TΦT–$(PTMO_{1000}/DMT)_{2000}$; (2000(1000)i) TΦT–$(PTMO_{1000}/DMI)_{2000}$; and (2000m) TΦT–$PTMO_{2000m}$.

should be realized that the intensity of the X-ray beam varied between the different experiments and therefore the absolute values of the intensities should not be compared. As expected, TΦT–$PTMO_{2900}$ shows two distinct PTMO peaks and for TΦT–$PTMO_{2000}$ these peaks are also visible. In TΦT–$PTMO_{1000}$ and TΦT–$PTMO_{2000m}$ one broad PTMO peak is present, indicating that in these polymers the PTMO crystalline phase is not yet fully developed and that it is less ordered. The separate PTMO peaks start to develop for TΦT–$(PTMO_{1000}/DMT)_{2000}$ and TΦT–$(PTMO_{1000}/DMI)_{2000}$ at 1000% strain. The synchrotron WAXS measurements suggest that the PTMO (strain induced) crystallinity increases approximately in the following direction: $PTMO_{1000} < PTMO_{2000m} < (PTMO_{1000}/DMT)_{2000}$, $(PTMO_{1000}/DMI)_{2000} < PTMO_{2000} < PTMO_{2900}$.

In Table 4, the values for T_m and ΔH_m of the PTMO phase of several unoriented and oriented polymers is given. Combining the DSC and WAXS observations, it is concluded that $PTMO_{1000}$ based soft segments and $PTMO_{2000m}$ undergo reversible strain induced crystallization, i.e. they crystallize during straining, but melt when the strain is released. This phenomenon is also observed for some rubbers such as *cis*-polybutadiene and *cis*-polyisoprene [29,30]. PTMO segments of 2000 g/mol and longer strain crystallize irreversibly.

3.5. PTMO orientation

The PTMO orientation can be quantified from the synchrotron WAXS measurements by determination of the half width of the angular intensity distribution curve of the PTMO 020 ($d = 4.4$ Å) reflection (Eq. (4)). For a good comparison between the different types of PTMO the orientation factor can only be applied if separate PTMO peaks can be distinguished, which in most cases starts at a strain of approximately 500%. In Fig. 14 the orientation of the different PTMO segments in the polymers is shown. The PTMO orientation increases upon straining and hardly any differences between the different types of PTMO are observed. $PTMO_{2000}$ has a somewhat higher orientation than the other types of PTMO, especially at strains above 1000%. This might be attributed to the higher crystallinity of $PTMO_{2000}$. Maybe the distribution of the orientation values is smaller in the crystalline fraction than in the amorphous fraction leading to a higher overall orientation value for a sample with a higher PTMO crystallinity.

With IR-dichroism hardly any PTMO orientation during the first 500% strain was observed (Fig. 6). The synchrotron WAXS measurements show that most of the PTMO orientation occurs after 500% strain. The small orientation observed in the first 500% (IR-dichroism) disappeared upon load release. Synchrotron WAXS measurements were carried out to see whether the PTMO orientation induced at strains above 500% also disappears after load release. In Fig. 15 three WAXS pictures of oriented TΦT–$(PTMO_{1000}/DMT)_{2000}$ fibers (drawn to 750%) are shown. Fig. 15a is the drawn fiber, Fig. 15b is the drawn fiber measured at 200% strain and Fig. 15c is the same fiber 30 min after strain release. Comparing Fig. 9b and c with Fig. 15a it can be concluded that part of the PTMO orientation and crystallization that is induced during straining disappeared upon load release. If the strain is applied again to the drawn fiber, the PTMO orientation immediately returns (Fig. 15b). In Table 5 the orientation factors (O) of the PTMO phase for several oriented polymers, before, during and after straining and of the corresponding unoriented fiber strained to 730% are given. All the polymers possess a more oriented PTMO phase during straining than in the relaxed state. Except for TΦT–$PTMO_{2000}$, the PTMO

Table 4
PTMO melting temperature ($T_{m,s}$) and heats of melting ($\Delta H_{m,s}$) of unoriented and oriented (1000% pre-strained) polymers (subscript s refers to soft segment)

Polymer	Unoriented		After straining 1000%	
	$T_{m,s}$ (°C)	$\Delta H_{m,s}$ (J/g)	$T_{m,s}$ (°C)	$\Delta H_{m,s}$ (J/g)
TΦT–$PTMO_{1000}$	–	–	–	–
TΦT–$PTMO_{2000}$	−3	27	43	28
TΦT–$PTMO_{29000}$	−2	24	47	43
TΦT–$PTMO_{2000\ m}$	−25	12	−18	13
TΦT–$(PTMO_{1000}/DMT)_{2060}$	−5	17	−4	13
TΦT–$(PTMO_{1000}/DMT)_{2055}$	−9	15	−6	13

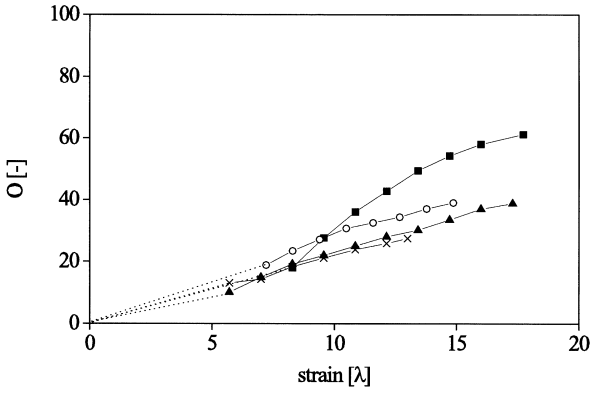

Fig. 14. PTMO orientation ($d = 4.34$ Å) for: (■) TΦT–$PTMO_{2000}$; (○) TΦT–$PTMO_{2000m}$; (×) TΦT–$(PTMO_{1000}/DMT)_{2000}$; and (▲) TΦT–$(PTMO_{1000}/DMI)_{2000}$.

orientation of the oriented and strained fiber is comparable to the orientation at 730% strain starting from the unoriented polymer. For TΦT–$PTMO_{2000}$, the PTMO orientation of the oriented and strained fiber is even higher than the orientation of the unoriented fiber strained to 730%. For TΦT–$(PTMO_{1000}/DMT)_{2000}$ the PTMO orientation of the oriented, strained, but relaxed fiber, was the same as the orientation of the oriented fiber before straining. These results indicate that the PTMO orientation that is induced upon straining is lost as soon as the strain is released.

4. Conclusion

TΦT–PTMO copolymers possess a two-phase structure: extremely thin TΦT lamellae (1.8 nm) physically crosslink

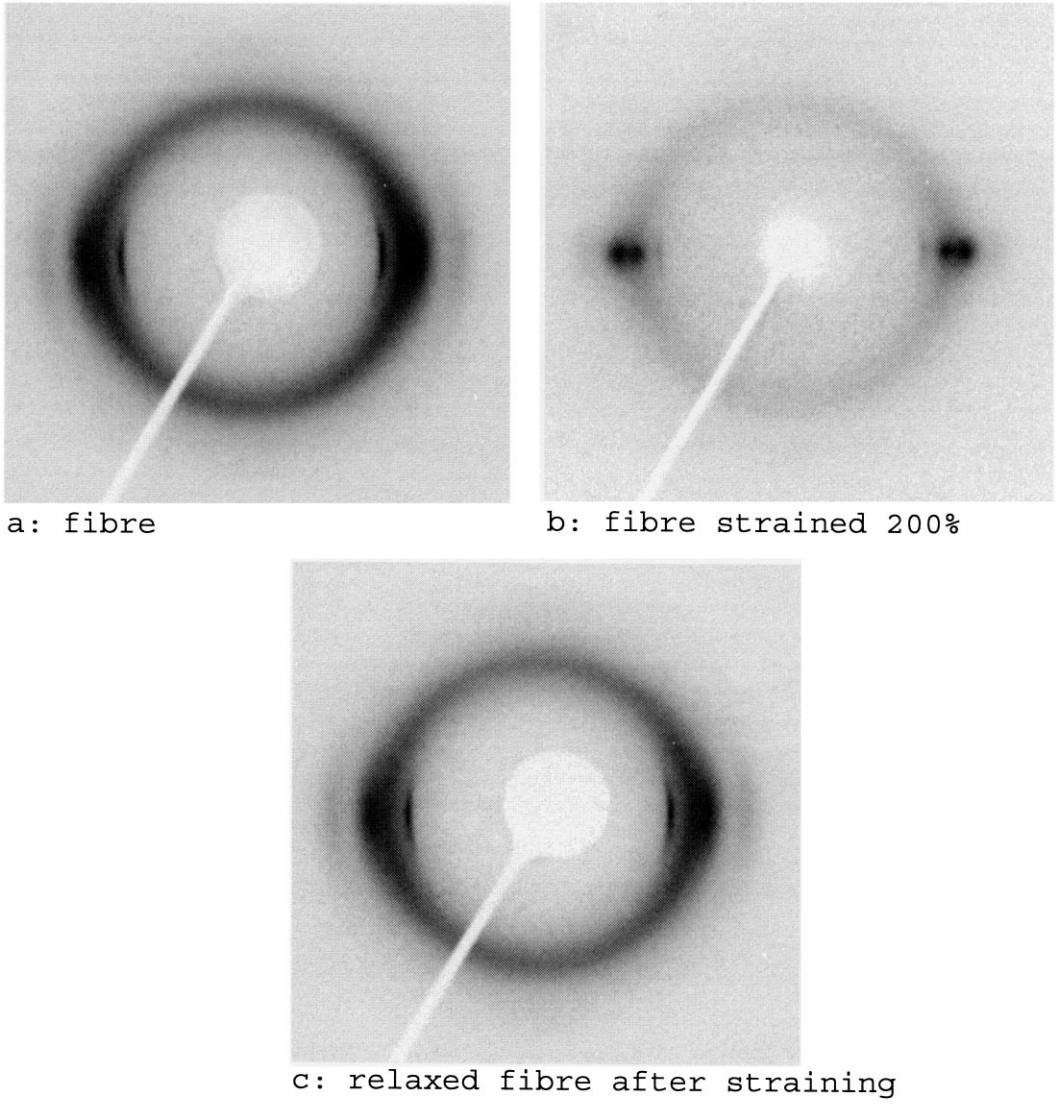

Fig. 15. Synchrotron WAXS pictures of oriented TΦT–$(PTMO_{1000}/DMT)_{2000}$.

Table 5
Orientation (O) of PTMO phase ($d = 4.34$ Å) for several oriented and unoriented polymers

	Oriented fiber, drawn to 750%			Unoriented fiber
Polymer	No strain	Strained (200%)	30 min after strain release	Strained (730%)
TΦT–$PTMO_{2000}$	–	75	19	19
TΦT–$(PTMO_{1000}/DMT)_{2000}$	5	20	5	18
TΦT–$(PTMO_{1000}/DMT)_{2000}$	–	20	5	19
TΦT–$(PTMO_{1000}/DMT)_{3000}$	–	16	4	26
TΦT–$PTMO_{2000\ m}$	–	16	5	23

the PTMO amorphous phase. The TΦT units self-assemble in the melt through the formation of hydrogen bonds forming a possible smectic-crystalline phase. With IR-dichroism a perpendicular orientation of the TΦT lamellae was observed during the first 300% strain. At higher strains, the orientation becomes parallel. The following model for the structural changes during deformation was proposed: first the TΦT crystalline network is disrupted and the lamellae are, due to their high aspect ratio, preferentially oriented perpendicular to the polymer chain direction. At the same time, the TΦT lamellae are broken up in their lateral dimension into eventually square crystallites. These small crystallites are oriented parallel to the polymer chain direction.

After approximately 300% strain, the polyether phase strain crystallizes. The TΦT orientation is irreversible while the PTMO orientation disappears upon strain release. $PTMO_{1000}$ based soft segments and PTMOm soft segments strain crystallize reversibly and linear PTMO segments longer than 1000 g/mol strain crystallize irreversibly.

References

[1] Niesten MCEJ, Feijen J, Gaymans RJ. Polymer 2000;41:8487–500.
[2] Niesten MCEJ, Ten Brinke JW, Gaymans RJ. Polymer 2000 (in press).
[3] Niesten MCEJ, Gaymans RJ. Submitted for publication.
[4] Cella RJJ. J Polym Sci: Symp 1973;42:727–40.
[5] Adams RK, Hoeschele GK. In: Legge NR, Holden G, Schroeder HE, editors. Thermoplastic elastomers, 1st ed. Munich: Hanser, 1987 (chap. 8).
[6] Van Hutten P, Walch E, Veeken AHM, Gaymans RJ. Polymer 1990;31:524–9.
[7] Sek D, Wolinska A, Janeczek H. J Polym Mater 1986;3:225–34.
[8] Lenz RW. Polym J 1985;17(1):105–15.
[9] Kricheldorf HR, Probst N, Schwarz G, Wutz C. Macromolecules 1996;29:4234–40.
[10] Wutz C. Polymer 1998;39(1):1–6.
[11] Bonart R. J Macromol Sci-Phys 1968;B2(1):115–38.
[12] Allegrezza AE, Seymour RW, Ng HN, Cooper SL. Polymer 1973;15:433–40.
[13] Seymour RW, Allegrazza AE, Cooper SL. Macromolecules 1973;6:896–902.
[14] Lilaonitkul A, West JC, Cooper SL. J Macromol Sci-Phys 1976;B12(4):563–97.
[15] Bogart JWC, Lilaonitkul A, Lerner LE, Cooper SL. J Macromol Sci-Phys 1980;B17(2):267–301.
[16] Ward IM. Structure and properties of oriented polymers. 2nd ed. London: Chapman and Hall, 1997 (chap. 2).
[17] Moreland JC, Wilkes GL. J Appl Polym Sci 1991;43:801–15.
[18] www.esrf.fr/exp_facilities/ID11/handbook/welcome.html.
[19] Van Bennekom ACM, Gaymans RJ. Polymer 1997;38(3):657–66.
[20] Northolt MG. Eur Polym J 1974;10:779–804.
[21] Harkema S, Gaymans RJ. Acta Crystallogr 1977;B33:3609–11.
[22] Skrovanek DJ, Howe SE, Painter PC, Coleman MM. Macromolecules 1985;18(9):1676–83.
[23] Geiger W. Spectrochim Acta 1966;22:495–9.
[24] Hiemenz PC. Polymer chemistry, the basic concepts. New York: Marcel Dekker, 1984 (chap. 4).
[25] Cesari M, Perego G, Mazzei A. Die Makromol Chemie 1964;61:197–206.
[26] Yamada K, Hashimoto K, Takayanagi M. J Appl Polym Sci 1987;33:1649–61.
[27] Krigbaum WR, Dawkins JV, Via GH, Balta YI. J Polym Sci, Part A 1966;4:475–89.
[28] Abhiraman AS. Proc R Soc London, A 1997;453:1649–50.
[29] Treloar LGR. The physics of rubber elasticity. 3rd ed. Oxford: Clarendon Press, 1975 (chap. 1).
[30] Sperling LH. Introduction to Physical Polymer Science. 2nd ed. New York: Wiley, 1992 (chap. 9).